arXiv:1602.03809v1 [physics.chem-ph] 11 Feb 2016

Consistent Interpretation of Molecular Simulation Kinetics Using Markov State Models Biased with External Information

Joseph F. Rudzinski,[1, a)] Kurt Kremer,[1] and Tristan Bereau[1]
Max Planck Institute for Polymer Research, 55128 Mainz, Germany

Molecular simulations can provide microscopic insight into the physical and chemical driving forces of complex molecular processes. Despite continued advancement of simulation methodology, model errors may lead to inconsistencies between simulated and reference (e.g., from experiments or higher-level simulations) observables. To bound the microscopic information generated by computer simulations within reference measurements, we propose a method that reweights the microscopic transitions of the system to improve consistency with a set of coarse kinetic observables. The method employs the well-developed Markov state modeling framework to efficiently link microscopic dynamics with long-timescale constraints, thereby consistently addressing a wide range of timescales. To emphasize the robustness of the method, we consider two distinct coarse-grained models with significant kinetic inconsistencies. When applied to the simulated conformational dynamics of small peptides, the reweighting procedure systematically improves the timescale separation of the slowest processes. Additionally, constraining the forward and backward rates between metastable states leads to slight improvement of their relative stabilities and, thus, refined equilibrium properties of the resulting model. Finally, we find that difficulties in simultaneously describing both the simulated data and the provided constraints can help identify specific limitations of the underlying simulation approach.

Despite acknowledged limitations in current all-atom (AA) force fields to describe complex molecular systems (e.g., proteins[1,2]), the confidence associated with atomically-detailed molecular dynamics simulations continues to increase.[3] This can be attributed to improvements in simulation models[4–7] and methodologies,[8–12] as well as continued experimental validation.[13,14] The latter has been facilitated by both increased resolution of experiments[15–18] and improved tools[19–22] for comparing simulated and measured data. Beyond ongoing improvements of simulation models, the microscopic insight extracted from existing simulations can be refined by altering the trajectories to improve their agreement with external data.[23,24] For example, Beauchamp *et al.*[25] recently proposed a method to reweight the ensemble of peptide configurations generated from a molecular dynamics simulation to be consistent with experimental chemical shift and ^3J measurements, leading to a systematic improvement of secondary-structure propensities.

Expanding upon this idea, the present work proposes a method to improve the kinetic properties determined from a simulation, given a set of reference observables. We seek to relate the microscopic transitions of the system with much coarser observables, effectively linking a wide range of timescales. Practically, this link is provided by Markov state models (MSMs), which describe the long-time dynamics of a system with a memoryless evolution of microstate transitions. The methodology for constructing MSMs directly from simulations has been extensively developed[26–34] and MSMs are routinely employed to elucidate complex simulated processes, e.g., protein folding[35–40] and protein-ligand binding.[41–45] Additionally, recent work[46] has applied MSMs to identify various discrepancies in the dynamical properties generated by different AA force fields. By incorporating simulation data as well as experimental kinetic constraints, the proposed method may provide insight into the relevance and source of such discrepancies. Moreover, the approach may be particularly useful to characterize the relationship between dynamics generated by AA and coarse-grained (CG) models. This relationship is generally not well understood, limiting the applicability of a large number of CG models to static equilibrium properties.[47,48]

An MSM is fully characterized by a transition probability matrix, $\mathbf{T}(\tau)$, whose elements, T_{ij}, describe the probability of jumping from microstate i to j within a "lag time" τ. The number of observed jumps between each pair of microstates during a simulation determines the count matrix, $\mathbf{C}^{\rm obs}(\tau)$. An MSM that accurately describes the long-time simulation dynamics may be constructed by maximizing the log-likelihood function $Q(\mathbf{T}) = \ln p(\mathbf{T} \mid \mathbf{C}^{\rm obs})$, where the probability of the model given the simulation data is[37]

$$p(\mathbf{T} \mid \mathbf{C}^{\rm obs}) \propto p(\mathbf{C}^{\rm obs} \mid \mathbf{T}) = \prod_{ij} T_{ij}^{C_{ij}^{\rm obs}} . \qquad (1)$$

The proportionality follows from Bayes' theorem, while the rightmost expression is implied by Markovian dynamics. The resulting maximum likelihood estimate (mle), $\mathbf{T}^{\rm mle}$, represents the MSM most likely to generate $\mathbf{C}^{\rm obs}$. Physical constraints, e.g., detailed balance, are typically incorporated[49] into the optimization of $\mathbf{T}^{\rm mle}$ in order to overcome finite sampling errors of the simulation. Moreover, convex optimization routines[37] can efficiently determine $\mathbf{T}^{\rm mle}$ for MSMs with hundreds of microstates.[45]

In the present work, we consider the mle problem (Eq. 1), while incorporating kinetic constraints, $\mathscr{F}(\mathbf{T}) = 0$, between macrostates (i.e., collections of microstates). Unfortunately, these constraints are, in general, nonlinear functions of the elements T_{ij}, preventing the straight-

a)Electronic mail: rudzinski@mpip-mainz.mpg.de

forward application of Lagrange multipliers or the use of convex optimization routines.[50] Furthermore, a simulation model may prove incompatible with $\mathscr{F}(\mathbf{T})$, such that strict enforcement would destroy much of the microscopic information provided by the trajectory. As such, we seek to maximize the agreement with the constraints while minimally biasing the original MSM (i.e., $\mathbf{T}^{\mathrm{mle}}$). We achieve this balance with Metropolis Monte Carlo sampling of transition probability matrices according to

$$E_{\mathrm{tot}}(\mathbf{T} \mid \lambda) = \lambda E_Q(\mathbf{T}) + (1-\lambda) E_{\mathscr{F}}(\mathbf{T}), \qquad (2)$$

where the energies $E_Q(\mathbf{T})$ and $E_{\mathscr{F}}(\mathbf{T})$ are shifted and rescaled quantities with respect to $\mathrm{Q}(\mathbf{T})$ and $\mathscr{F}(\mathbf{T})$, respectively.[51] These quantities are defined such that $E_Q(\mathbf{T}^{\mathrm{mle}}) = 0$, $E_{\mathscr{F}}(\mathbf{T}) = 0$ when $\mathscr{F}(\mathbf{T}) = 0$, and $\max(E_Q(\mathbf{T}))$, $\max(E_{\mathscr{F}}(\mathbf{T})) \approx 1$ for the relevant range of sampled matrices. The control parameter, λ, balances the contribution of the two quantities. In practice, we monitor the two energy terms while tuning λ in order to determine the optimal "biased" MSM. We note that when $\lambda = 1$ the scheme provides the uncertainty of $\mathbf{T}^{\mathrm{mle}}$.[49,52,53] While we include additional technical details in the Supporting Information,[51] we leave a detailed assessment to a subsequent publication. All MSM calculations employed an inhouse extension of the PyEmma package.[54,55]

We apply the proposed method to the conformational dynamics of two small peptides. For each system, we consider simulations of both an AA and a CG model. To illustrate the robustness of the method, we consider a highly specific bottom-up model for one system while using a more transferable top-down model for the other. CG models, which lump several atoms into a single CG site, often display faster dynamics than a corresponding AA model due to reduced molecular friction between sites. As a consequence, these models are excellent candidates to test the present methodology.

For each system, we compare three distinct MSMs constructed from the simulations: (1) the "ref" model: an unbiased MSM constructed using AA data; (2) the "UMSM": an unbiased MSM constructed using CG data; and (3) the "BMSM": a biased MSM constructed via Monte Carlo sampling according to Eq. 2, which incorporates CG simulation data as well as external constraints. The chosen constraints involve mean first passage times (MFPTs), $\{m_K\}$, between metastable states determined from the ref model. The MFPTs are calculated directly from $\mathbf{T}$ by solving a set of linear equations.[54,55] Here, the ref model allows a detailed assessment of the properties of the UMSM and BMSM. In general, however, a reference MSM is unnecessary, since the procedure requires only coarse (e.g., macrostate-level) information.

As expected, the CG models displayed significantly faster dynamics than the underlying AA model, allowing enhanced sampling at reduced computational expense. Ideally, a CG model should retain enhanced dynamics while consistently or predictably speeding up all relevant kinetic processes. To this end, we consider only ratios of MFPTs: $\tilde{m}_K \equiv m_K/m_{\mathrm{L}}$, where K denotes a (directional) transition between two metastable states and L denotes the particular transition corresponding to the longest MFPT of the ref model. We set the constraint as the root sum square of relative errors of MFPT ratios, $\mathscr{F} = \sqrt{\sum_K \left(\tilde{m}_K - \tilde{m}_K^{\mathrm{ref}}\right)^2 / \left(\tilde{m}_K^{\mathrm{ref}}\right)^2}$. Thus, we aim to recover the dynamics of the system up to a *homogeneous* speedup factor, which requires $\mathscr{F} = 0$. We circumvent a calibration of the AA and CG timescales by only comparing the eigenvalues of the MSMs, $\{\lambda_j\}$, which are linked to the timescales of particular processes $\{j\}$ by $t_j = -\tau/\ln\lambda_j$.[31] Due to the ambiguity of the CG dynamics, we report CG timescales in reduced units, $\mathcal{T}^{\mathrm{CG}}$, specific to the model.

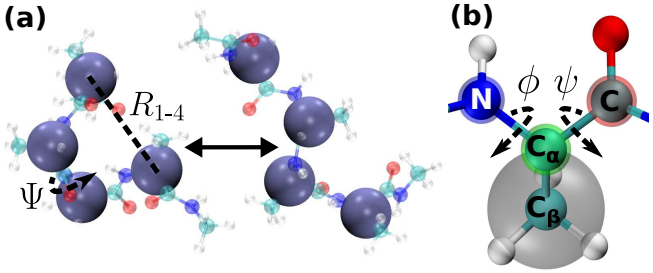

FIG. 1. Representation and relevant degrees of freedom of the CG models for (a) Ala_4 and (b) Ala_3. Rendered with VMD.[56]

We first considered a tetra-peptide of alanine residues (Ala_4). The AA simulation employed the OPLS-AA[57] and SPC/E[58] force fields to model an explicitly solvated, capped Ala_4 peptide. The CG simulation employed a structure-based force field,[59] which represents each amino acid with a single CG site placed at the α-carbon position, to model an implicitly solvated Ala_4 peptide. This model qualitatively reproduces the free-energy surface (FES) along the dihedral angle, Ψ, defined between the four α-carbons of the peptide backbone and the end-to-end distance, $R_{1\text{-}4}$, between the first and last α-carbons (Fig. 1a). The simulation and parameterization details were previously published.[59] Both AA and CG trajectories were discretized on a uniform grid along Ψ and $R_{1\text{-}4}$. MSMs were constructed with lag times of $\tau = 250$ ns and 1.25 $\mathcal{T}^{\mathrm{S}}$ for the AA and CG models, respectively, where $\mathcal{T}^{\mathrm{S}}$ denotes the time unit for the structure-based model.

	(a) Ala_4	(b) Ala_3	
	H - E	α - β	α_{L} - β
ref	0.51	0.42	4.18
UMSM	0.96	0.95	5.75
BMSM	0.88	0.75	5.73

TABLE I: Free-energy differences (in units of $k_{\mathrm{B}}T$) with respect to the most stable metastable state for (a) Ala_4 and (b) Ala_3.

Fig. 2 compares the FESs along Ψ and $R_{1\text{-}4}$ determined from the ref model (panel a) and the UMSM (panel c). Additionally, panel b presents two metastable states, de-

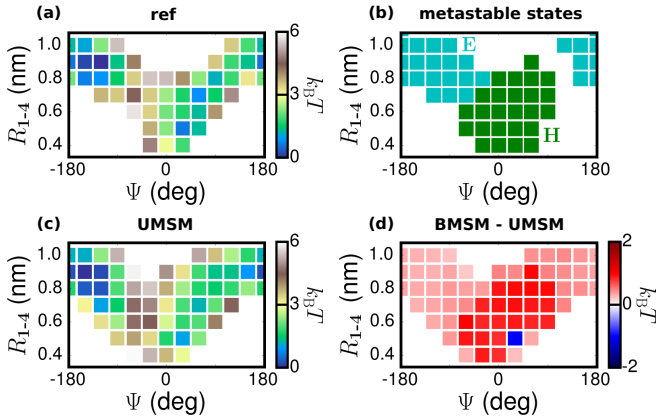

FIG. 2. Ala_4. Free-energy surfaces of Ala_4 along Ψ and $R_{1\text{-}4}$ determined from the (a) ref model, (c) UMSM, and (d) difference between the BMSM and UMSM. (b) Helical (H, green) and extended (E, cyan) metastable states.

termined from the ref model via the PCCA+ algorithm,[60] corresponding to helical (H, green) and extended (E, cyan) structures. The AA model connects these two regions through intermediates with $\Psi \approx 130$ deg and $R_{1\text{-}4} \approx 0.9$ nm. While it is possible to describe the transition in more detail, we only consider these two states to focus on the description of the slowest process. Table Ia presents the free-energy difference between the H and E states for each model. Despite the apparent structural agreement of the FESs, the free-energy difference between the metastable states is significant.

Fig. 3 demonstrates that there are also significant discrepancies in the kinetic properties of the UMSM. We first probe the accuracy of the ratios of MFPTs between the metastable states, which will be employed as constraints in the construction of the BMSM. This agreement is assessed by calculating the relative fractional speedup, Γ, of each MFPT: $\Gamma(m_K) \equiv \tilde{m}_K/\tilde{m}_K^{\text{ref}}$. Deviations from $\Gamma = 1$ indicate discrepancies in the MFPTs, beyond a homogeneous speedup factor. The solid blue line in Fig. 3a demonstrates that the H → E transition is too fast compared to the reverse process in the UMSM.

The kinetic properties of the UMSM are further characterized from the eigenvalues and eigenvectors of the transition probability matrix. Fig. 3b presents the largest four eigenvalues of each model. For any MSM of a system at equilibrium, the largest eigenvalue is $\lambda_0 = 1$ and its eigenvector coincides with the equilibrium probability distribution.[31] The remaining eigenvectors describe the slowest processes of the system, sorted by their eigenvalue. Fig. 3c presents the eigenvector of λ_1 for each model, which describes a flux of the probability distribution between microstates with positive and negative values, weighted by the individual eigenvector component of each microstate. The UMSM properly describes the transition between the two metastable states, likely due to the careful parametrization of the CG model.[59] On the other hand, Fig. 3b demonstrates that the UMSM does not reproduce the implied separation of timescales between indices 1 and 2 of the ref model.

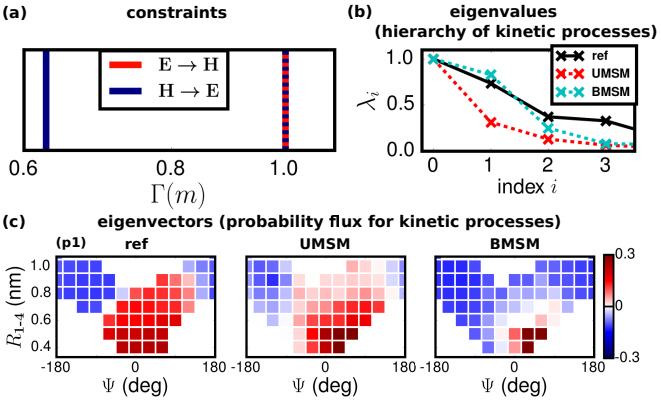

FIG. 3. Ala_4. (a) Relative fractional speedup, Γ (defined in text), of each MFPT for the UMSM (solid lines) and BMSM (dashed lines); (b) 4 largest eigenvalues; and (c) Eigenvector characterizing the slowest dynamical process (λ_1) of each model. The intensity plots describe a flux of probabilities between microstates with positive and negative values, weighted by the magnitude of the individual components.

Starting with the UMSM, the constraint function, $\mathscr{F}$, built from the MFPT ratios between states H and E, was applied to sample transition matrices according to Eq. 2. From the ensemble of MSMs approximately fulfilling the constraint, an optimal BMSM, sampled with $\lambda = 0.875$, was chosen to balance $E_Q(\mathbf{T})$ and $E_{\mathscr{F}}(\mathbf{T})$ (see Fig. S7[51]). The blue dashed line in Fig. 3a demonstrates that the resulting BMSM nearly quantitatively reproduces the given constraint, i.e., $\Gamma(m_{\text{E}\to\text{H}}) \approx 1$. The BMSM yields a larger separation of timescales (Fig. 3b), in much better agreement with the ref model. However, the description of the slowest process (Fig. 3c) is somewhat degraded, with increased probability flux in a narrow region of H. At the same time, the most probable microstate in this region is significantly stabilized (Fig. 2d).

The non-uniform distribution of probability flux characterizing the H to E transition is already apparent in the UMSM's description of process 1 (Fig. 3c). Moreover, further analysis (Fig. S7 and S8[51]) indicates that this feature is not an artifact of sampling but, rather, emerges systematically from the combined application of the CG simulation and reference data to construct the BMSM. In Eq. 2, E_Q ensures the essential dynamical features of the underlying simulation are minimally perturbed. The inclination of the BMSM to reproduce the MFPTs and timescale separation by exacerbating the concentrated probability flux of the helical region implicates this non-uniform flux as an essential component of the underlying simulated processes.

Interestingly, previous work demonstrated that the CG interaction potentials of this model stabilize helical transitions through strong, non-cooperative interactions in order to compensate for the presence of conformations sterically forbidden in the AA model.[59] This feature ap-

pears to give rise to a transition from helix to extended structures that is inherently more localized within the helical state, leading to the heterogeneous flux profiles observed in the CG MSMs. Although further investigation is required to clarify the precise connection between these features, this analysis strongly implicates the methodology as a useful tool for identifying inherent limitations in the underlying simulation model.

As a second example, we also considered a tri-alanine peptide (Ala_3). The AA simulation employed the same model and implementation as described above for Ala_4. The CG simulation employed the top-down PLUM force field,[61] which represents each heavy atom of the peptide backbone as well as each side chain with a CG site, to model an implicitly solvated Ala_3 peptide. Both trajectories were discretized on a uniform grid along the ϕ and ψ dihedral angles of the center residue (Fig. 1b). MSMs were then constructed with lag times of $\tau = 40$ ns and 1.5 $\mathcal{T}^{\mathrm{P}}$ for the AA and CG models, respectively, where $\mathcal{T}^{\mathrm{P}}$ denotes the time unit for the PLUM model.

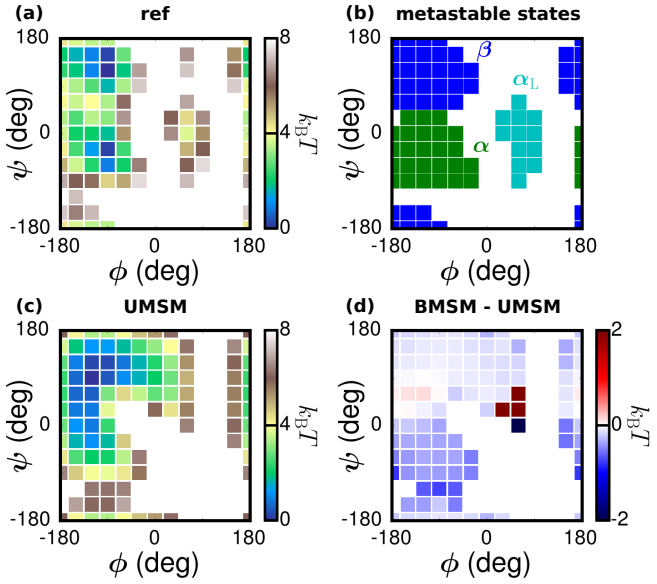

FIG. 4. Ala_3. Free-energy surfaces of Ala_3 along the ϕ and ψ dihedral angles determined from the (a) ref model, (c) UMSM, and (d) difference between the BMSM and UMSM. Panel (b) presents the definition of the three metastable states: corresponding to alpha-helical (α, green), beta-sheet (β, blue), and left-handed-helical (α_{L}, cyan) regions.

Fig. 4 compares FESs along ϕ and ψ determined from the ref model (panel a) and the UMSM (panel c). Additionally, panel b presents three metastable states, determined from the ref model via the PCCA+ algorithm,[60] corresponding to alpha-helical (α, green), beta-sheet (β, blue), and left-handed-helical (α_{L}, cyan) structures. Panel c shows that the CG model samples the metastable states with incorrect propensities (quantified in Table Ib). In terms of kinetics, the solid lines in Fig. 5a indicate that the timescales of transition between the metastable states differ qualitatively from the ref model, beyond a homogeneous speedup factor. In this case, Γ is determined relative to the $\alpha \to \alpha_{\mathrm{L}}$ transition. Fig. 5b demonstrates that the UMSM does not reproduce the implied separation of timescales between indices 2 and 3. Worse still, because λ_1 and λ_2 are nearly degenerate, the hierarchy of kinetic processes cannot be reliably determined. In this case, the order of these processes is qualitatively different from the ref model (Fig. 5c). While the two slowest processes of the ref model (column 1) correspond to transitions involving α_{L} and between α and β, the processes of the UMSM (column 2) are in reverse order and significantly skewed.

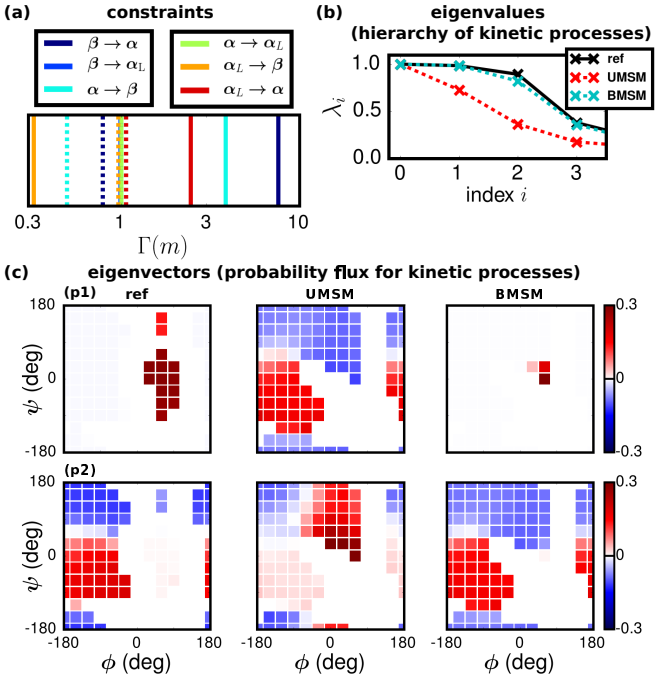

FIG. 5. Ala_3. (a) Relative fractional speedup, Γ (defined in text), of each MFPT for the UMSM (solid lines) and BMSM (dashed lines); (b) 4 largest eigenvalues; and (c) Eigenvectors characterizing the two slowest dynamical processes, λ_1 (p1) and λ_2 (p2) of each model. (Negative values are too small to be noticed in p1 ref and BMSM).

Similar to Ala_4, the constraint $\mathscr{F}$, characterizing the error in the MFPT ratios between metastable states, was applied to sample MSMs according to Eq. 2. An optimal BMSM was identified as described above for Ala_4, sampled with $\lambda = 0.9$ (see Fig. S10[51]). In this case, the constraints could not be perfectly fulfilled without significantly deteriorating agreement with the simulation data. The dashed lines in Fig. 5a quantify this discrepancy. Fig. 4d demonstrates the BMSM's pronounced, but localized, adjustments of microstate stabilities in the α_{L} region, although the overall stability remains largely unchanged (Table Ib). The BMSM also slightly destabilizes the interface region between the α and β metastable states, while providing an overall stabilization of both regions, resulting in a significantly improved free-energy

difference (Table Ib). These adjustments result in relative fractional speedups much closer to 1 (Fig. 5a, dashed lines) as well as excellent agreement in the separation of timescales (Fig. 5b). Moreover, not only do the first two eigenvectors more accurately describe the underlying processes, but the hierarchy is also restored (Fig. 5c).

This work outlines a simple method to determine an MSM that combines information from a computer simulation with a set of kinetic constraints. Importantly, the scheme does not severely restrict the form of the constraint, allowing experimental measurements to inform the construction of the model. The proposed framework also allows simple and transparent flexibility in the enforcement of the constraints. Indeed, we find that the optimal model may not perfectly reproduce the given constraints. For the conformational dynamics of two small peptides, the BMSM improves the description of kinetics, both in terms of the constrained MFPTs and the implied timescales associated with the slowest processes, while refining slightly but systematically the equilibrium distribution of the metastable states.

In the context of CG models, the method provides a systematic framework to interpret kinetic properties in a meaningful and consistent way. We plan to investigate the transferability of micro-trajectory reweighting beyond the system used in the original calculation. Interestingly, we find that the BMSM may exacerbate artifacts of the underlying model, implicating the method as a potential tool for the refinement of molecular force fields, in the case that an underlying model is available. Finally, we expect the method will also be useful for investigations comparing high-resolution AA simulations and experimental measurements of complex biomolecular processes, e.g., protein folding.

ACKNOWLEDGMENTS

The authors thank Will Noid for the use of the Ala_4 simulation trajectories. We thank Denis Andrienko, Cristina Greco, and Marc Radu for critical reading of the manuscript and Benjamin Trendelkamp-Schroer for insightful discussions concerning MSM methodology. J.F.R. and T.B. are also thankful to the organizers and participants of the 2015 Winter School on Markov State Models and Molecular and Chemical Kinetics conference. Funding from the SFB-TRR146 grant of the German Research Foundation (DFG) is gratefully acknowledged.

REFERENCES

[1] R. B. Best, N.-V. Buchete, and G. Hummer, Biophys. J. **395**, L07 (2008).
[2] E. A. Cino, W.-Y. Choy, and M. Karttunen, J. Chem. Theor. Comp. **8**, 2725 (2012).
[3] K. A. Beauchamp, Y.-S. Lin, R. Das, and V. S. Pande, J. Chem. Theor. Comp. **8**, 1409 (2012).
[4] R. B. Best and G. Hummer, J. Phys. Chem. B **113**, 9004 (2009).
[5] K. Lindorff-Larsen, S. Piana, K. Palmo, P. Maragakis, J. L. Klepeis, R. O. Dror, and D. E. Shaw, Prot. Struct. Func. Bioinfo. **78**, 1950 (2010).
[6] R. B. Best, X. Zhu, J. Shim, P. E. M. Lopes, J. Mittal, M. Feig, and A. D. MacKerell Jr., J. Chem. Theor. Comp. **8**, 3257 (2012).
[7] F. Jiang, W. Han, and Y.-D. Wu, Phys. Chem. Chem. Phys. **15**, 3413 (2013).
[8] D. E. Shaw, P. Maragakis, K. Lindorff-Larsen, S. Piana, R. O. Dror, M. P. Eastwood, J. A. Bank, J. M. Jumper, J. K. Salmon, Y. B. Shan, and W. Wriggers, Science **330**, 341 (2010).
[9] D. M. Zuckerman, in *Annual Review of Biophysics, VOL 40*, Annual Review of Biophysics, Vol. 40, edited by Rees, DC and Dill, KA and Williamson, JR (Annual Reviews, 2011) pp. 41–62.
[10] P. R. L. Markwick and J. A. McCammon, Phys. Chem. Chem. Phys. **13**, 20053 (2011).
[11] H. Fujisaki, K. Moritsugu, Y. Matsunaga, T. Morishita, and L. Maragliano, Frontiers in bioengineering and biotechnology **3** (2015).
[12] A. Morriss-Andrews and J.-E. Shea, in *Annual Review of Physical Chemistry, Vol 66*, Annual Review of Physical Chemistry, Vol. 66, edited by Johnson, MA and Martinez, TJ (Annual Reviews, 2015) pp. 643–666.
[13] O. F. Lange, D. van der Spoel, and B. L. de Groot, Biophys. J. **99**, 647 (2010).
[14] K. Lindorff-Larsen, P. Maragakis, S. Piana, M. P. Eastwood, R. O. Dror, and D. E. Shaw, PLoS ONE **7** (2012), 10.1371/journal.pone.0032131.
[15] D. Nettels, I. V. Gopich, A. Hoffmann, and B. Schuler, Proc. Natl. Acad. Sci. USA **104**, 2655 (2007).
[16] H. S. Chung, K. McHale, J. M. Louis, and W. A. Eaton, Science **335**, 981 (2012).
[17] H. Oikawa, Y. Suzuki, M. Saito, K. Kamagata, M. Arai, and S. Takahashi, Scientific Reports **3** (2013), 10.1038/srep02151.
[18] T. Otosu, K. Ishii, and T. Tahara, Nat. Commun. **6**, 7685 (2015).
[19] F. Noé, S. Doose, I. Daidone, M. Löllmann, M. Sauer, J. D. Chodera, and J. C. Smith, Proc. Natl. Acad. Sci. USA **108**, 4822 (2011).
[20] B. G. Keller, J.-H. Prinz, and F. Noé, Chem. Phys. **396**, 92 (2012).
[21] B. Lindner, Z. Yi, J.-H. Prinz, J. C. Smith, and F. Noé, J. Chem. Phys. **139**, 175101 (2013).
[22] Z. Yi, B. Lindner, J.-H. Prinz, F. Noé, and J. C. Smith, J. Chem. Phys. **139**, 175102 (2013).
[23] M. Groth, J. Malicka, C. Czaplewski, S. Oldziej, L. Lankiewicz, W. Wiczk, and A. Liwo, J Biomol NMR **15**, 315 (1999).
[24] B. Różycki, Y. C. Kim, and G. Hummer, Structure **19**, 109 (2011).
[25] K. A. Beauchamp, V. S. Pande, and R. Das, Biophys. J. **106**, 1381 (2014).
[26] J. D. Chodera, W. C. Swope, J. W. Pitera, and K. A. Dill, Multiscale Model. Simul. **5**, 1214 (2006).
[27] F. Noé, C. Schütte, E. Vanden-Eijnden, L. Reich, and T. R. Weikl, Proc. Natl. Acad. Sci. USA **106**, 19011 (2009).
[28] J.-H. Prinz, M. Held, J. C. Smith, and Noé, Multiscale Model. Simul. **9**, 545 (2011).
[29] J. D. Chodera and F. Noé, Curr. Opin. Struc. Biol. **25**, 135 (2014).
[30] F. Nüske, B. Keller, G. Pérez-Hernández, M. A., and F. Noé, J. Chem. Theor. Comp. **10**, 1739 (2014).
[31] Bowman, Gregory R. and Pande, Vijay S. and Noé, Frank, *An Introduction to Markov State Models and Their Application to Long Timescale Molecular Simulation* (Springer Science and Business Media, Dordrecht, Netherlands, 2014).
[32] H. Wu and F. Noé, J. Chem. Phys. **142**, 084104 (2015).
[33] C. Schütte and M. Sarich, Eur. Phys. J. Special Topics **224**, 2445 (2015).
[34] F. Vitalini, F. Noé, and B. G. Keller, J. Chem. Theor. Comp. **11**, 3992 (2015).

[35] J. D. Chodera, N. Singhal, V. S. Pande, K. A. Dill, and W. C. Swope, J. Chem. Phys. **126**, 155101 (2007).
[36] F. Noé, I. Horenko, C. Schütte, and J. C. Smith, J. Chem. Phys. **126** (2007), 10.1063/1.2714539.
[37] J.-H. Prinz, H. Wu, M. Sarich, B. Keller, M. Senne, M. Held, J. D. Chodera, C. Schütte, and F. Noé, J. Chem. Phys. **134**, 174105 (2011).
[38] J. D. Chodera and V. S. Pande, Proc. Natl. Acad. Sci. USA **108**, 12969 (2011).
[39] T. J. Lane, G. R. Bowman, K. Beauchamp, V. A. Voelz, and V. S. Pande, J. Am. Chem. Soc. **133**, 18413 (2011).
[40] G. R. Bowman, V. A. Voelz, and V. S. Pande, J. Am. Chem. Soc. **133**, 664 (2011).
[41] K. A. Beauchamp, D. L. Ensign, R. Das, and V. S. Pande, Proc. Natl. Acad. Sci. USA **108**, 12734 (2011).
[42] M. Held, P. Metzner, J.-H. Prinz, and F. Noé, Biophys. J. **100**, 701 (2011).
[43] I. Buch, T. Giorgino, and G. De Fabritiis, Proc. Natl. Acad. Sci. USA **108**, 10184 (2011).
[44] G. R. Bowman and P. L. Geissler, Proc. Natl. Acad. Sci. USA **109**, 11681 (2012).
[45] N. Plattner and F. Noé, Nat. Commun. **6**, 7653 (2015).
[46] F. Vitalini, A. S. J. S. Mey, F. Noé, and B. G. Keller, J. Chem. Phys. **142**, 84101 (2015).
[47] C. Peter and K. Kremer, Soft Matter **5**, 4357 (2009).
[48] W. G. Noid, J. Chem. Phys. **139**, 090901 (2013).
[49] F. Noé, J. Chem. Phys. **28**, 244103 (2008).
[50] R. Horst and P. M. Pardalos, *Handbook of Global Optimization* (Springer Science and Business Media, Dordrecht, Netherlands, 1995).
[51] See supplemental material at [URL will be inserted by AIP] for further technical details of the molecular simulations as well as Markov state model methodology and calculations.
[52] P. Metzner, F. Noé, and C. Schütte, Phys. Rev. E **80**, 1 (2009).
[53] P. Metzner, M. Weber, and C. Schütte, Phys. Rev. E **82**, 1 (2010).
[54] F. Noé and coworkers, "Pyemma," `https://github.com/markovmodel/PyEMMA/` (2015).
[55] M. Senne, B. Trendelkamp-Schroer, A. S. J. S. Mey, C. Schütte, and F. Noé, J. Chem. Theor. Comp. **8**, 2223 (2012).
[56] W. Humphrey, A. Dalke, and K. Schulten, J. Mol. Graph. **14**, 33 (1996).
[57] W. L. Jorgensen, D. S. Maxwell, and J. Tirado-Rives, J. Am. Chem. Soc. **118**, 11225 (1996).
[58] H. Berendsen, J. Grigera, and T. Straatsma, J. Phys. Chem. **91**, 6269 (1987).
[59] J. F. Rudzinski and W. G. Noid, J. Chem. Theor. Comp. **11**, 1278 (2015).
[60] P. Deuflhard and M. Weber, Linear Algebra Appl **398**, 161 (2005).
[61] T. Bereau and M. Deserno, J. Chem. Phys. **130**, 235106 (2009).